Polyhedron 27 (2008) 3112–3122

Contents lists available at ScienceDirect

Polyhedron

journal homepage: www.elsevier.com/locate/poly

Cyanometallate incorporated supramolecular networks based on a nitroalkyl-substituted $Cu^{II}N_4$ precursor: Synthesis, crystal structure, thermal and electrochemical studies

Ambarish Ray [a,1], Parikshit Chandra Mandal [b], Atish Dipankar Jana [c], William S. Sheldrick [d], Swastik Mondal [e], Monika Mukherjee [e], Mahammad Ali [a,*]

[a] Department of Chemistry, Jadavpur University, Kolkata 700 032, West Bengal, India
[b] Saha Institute of Nuclear Physics, Chemical Science Division, 1/AF Bidhan Nagar, Kolkata 700 064, India
[c] Department of Physics, Sripat Singh College, Jiaganj 700 032, West Bengal, India
[d] Lehrstuhl fur Analytischie Chemie, Ruhr-Universitat Bochum, D-44780 Bochum, Germany
[e] Department of Solid State Physics, Indian Association for the Cultivation of Science, Jadavpur, Kolkata 700 032, India

ARTICLE INFO

Article history:
Received 6 February 2008
Accepted 8 June 2008
Available online 20 August 2008

Keywords:
$Cu^{II}N_4$ precursor
Nitroalkyl pendant
Cyanometallate
Supramolecular networks
Electrochemical studies
Nitroradical anion

ABSTRACT

Two new copper(II) complexes, *viz.* $[Cu(nelin)(H_2O)_2]_2[Fe(CN)_6]\cdot 6H_2O$ (**2**) and $[\{Cu(nelin)\}_2Ni(CN)_4](ClO_4)_2\cdot 2H_2O$ (**3**), have been synthesized using $[Cu(nelin)](ClO_4)_2$ (**1**) (nelin = 1,9-diamino-5-methyl-5-nitro-3,7-diazanonane) as a nitroalkyl-substituted $Cu^{II}N_4$ precursor, and their structures and supramolecular networks have been fully explored using the single crystal X-ray diffraction technique. The H-bonded 1D chains of 2 run along the *a*-axis, being generated from supramolecular synthons using cations and anions, and are further propagated into a 3D array to form irregular honeycomb-like channels which are divided into two halves, with each half accomodating a helical water chain running in opposite directions to each other. In complex **3**, the trinuclear units are arranged in successive rows in a herring-bone fashion and bifurcated hydrogen bonding through the uncoordinated terminals of the $[Ni(CN)_4]^{2-}$ units give rise to a supramolecular (4,4) network. A comparison of the PXRD pattern of complex **2** and its dehydrated form indicate marked changes in the diffraction pattern with the development of a quasi glassy nature in the dehydrated form. The electrochemical properties of **1**, 2 and **3** have been investigated in comparative ways using the cyclic voltammetric technique in aqueous and MeCN solutions with Ag/AgCl as a reference electrode. Electrochemical reduction generates the one-electron reduced nitro-radical anion. In water–alcohol glass at 77 K complex **2** exhibits a typical four-line hyperfine EPR spectra with $g_{||} = 2.11$, $g_{\perp} = 2.02$, $A_{||} = 150$ Oe and $A_{\perp} = 5$ Oe at $\nu = 9.45$ MHz.

1. Introduction

Crystal engineering is a rapidly expanding global discipline practiced by scientists with diverse interests in modelling, synthesis, evaluation and utilization of crystalline solids; and research on materials with desired functions and fascinating topological architectures has become an area of increasing interest in recent years [1]. A reason for this interest is the synthetic strategy used to construct these materials with a high degree of design that may lead to the development of materials with (i) tunable properties including biomimetic structures, (ii) host–guest properties similar to those observed in zeolites and (iii) interesting electronic and magnetic properties [2]. A popular approach to the design and synthesis of such materials is to use cyanometallates $[M(CN)_x]^{n-}$ as building blocks [3] in conjugation with discrete metal ion complexes. Architectures of 1D, 2D or 3D networks [4] can be built up by suitably tuning the various cyanometallates as well as the metal complex nodes.

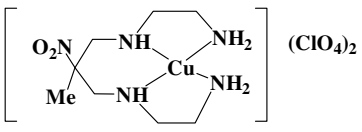

[Cu(Nelin)](ClO$_4$)$_2$ (1)

Though cyanometallate bridging between copper(II) precursors of selective bi- or tri- dentate N-donor ligands is relatively common [3,5], the corresponding networks under a $Cu^{II}N_4$ environment have been comparatively less explored [6]. The possible reasons may be due to the thermodynamic stability of the individual $Cu^{II}N_4$ square

* Corresponding author.
E-mail address: mali@chemistry.jdvu.ac.in (M. Ali).
[1] Present address: Department of Chemistry, A.B.N. Seal College, North Bengal University, Cooch-Behar 736 101, India.

0277-5387/$ - see front matter © 2008 Elsevier Ltd. All rights reserved.
doi:10.1016/j.poly.2008.06.035

planar moiety and also the reluctance to axial binding arising out of the Jahn–Teller effect.

In a continuation of our studies in this field [7], here we have strategically selected an N_4-donor copper(II) synthon, [Cu(nelin)]-$(ClO_4)_2$ (**1**) (nelin = 1,9-diamino-5-methyl-5-nitro-3,7-diazanonane) with a nitroalkyl pendant attached to the main ligand frame.

The utilization of such a precursor deserves special attention since nitro compounds are used extensively as antibacterial, antiprotozoal and anticancer agents [8]. Again, such compounds in metabolic pathways undergo a one-electron reduction to generate nitro-radical anions that exhibit cytotoxicity towards cellular systems [9], causing DNA damage within the cell. Furthermore, several nitro compounds [10] and some of their metal complexes [11] are potent radio-sensitizers towards hypoxic tumour cells, and the efficiency of these drugs is related to the one-electron reduction potential of these compounds [12]. It is therefore important to study the redox behavior of these nitro compounds and the reactivity of the corresponding one-electron reduced nitro-radical anions. So far, the reactivity of these nitro-radical anions has been studied mainly by pulse radiolysis [13] and in few cases by cyclic voltammetry [14], mostly in a mixed solvent medium. The cyclic voltammetric reduction of **1** [15] and other nitro compounds [16] in protic solvents at neutral pH resulted in a single irreversible cathodic wave corresponding to the four-electron reduction of the nitro group to the hydroxylamine derivative. Recently, cyclic voltammetric reduction of a heterocyclic drug, metronidazole, in aqueous solution and aqueous DMF [17] produced the nitro-radical anion successfully. However, monitoring of the redox behavior of copper(II) complexes containing a nitro group on a ligand fragment in vivo-friendly pure aqueous medium is absolutely a new era in this dimension.

In this paper attempts have been made to highlight two relevant aspects in a justified way. First we report the syntheses, crystal structures and other physical characterizations of two new cyano complexes viz. ionic $[Cu(nelin)(H_2O)_2]_2[Fe(CN)_6]\cdot 6H_2O$ (**2**) and bridged $[\{Cu(nelin)\}_2Ni(CN)_4](ClO_4)_2\cdot 2H_2O$ (**3**), by taking $[Cu(nelin)]^{2+}$ as the strategically starting synthon. It is noteworthy to mention here that cyanometallate incorporated copper(II) complexes in an N_4-donor diaza-diamine environment containing an $-NO_2$ pendant group has been scarcely studied [6e]. Here, the supramolecular view not only provides an aesthetically pleasing architecture, the simultaneous transformation of **2** to a quasi-glass phase on dehydration warrants special attention in material science. In the next part, we report the detailed comparative cyclic voltammetric studies of these compounds as well as the parent complex $[Cu(nelin)](ClO_4)_2$ (**1**), especially giving emphasis on the generation of the nitro-radical anion and its effects on the subsequent redox processes in pure aqueous and in MeCN media. In this regard, it is mentionable that the nitroalkyl-substituted $Cu^{II}N_4$ precursor and the cyanometallate incorporated complexes deserve further exploration in the context of the possibility of their potential application as radio-sensitizers in the treatment of cancer, as they are expected to serve in a better way than other organic drugs having poor solubility and high toxicity in physiological conditions compared to the macro-cyclic and acyclic complexes.

2. Experimental

2.1. Materials and methods

Materials such as aqueous formaldehyde (37%) (E-Merck, India), nitroethane (Aldrich), $HClO_4$, and $K_4[Fe(CN)_6]$ (E-Merck, India) were of reagent grade and were used as received. Ethylenediamine (E-Merck, India) and triethylamine (Ranbaxy, India) were distilled over sodium metal before use. Single distilled HPLC grade MeCN (Merck Germany) was used for the electrochemical studies. All the solutions of the complexes for the electrochemical studies were prepared freshly with double distilled water.

Elemental analyses were carried out using a Perkin–Elmer 240 elemental analyzer. Infrared spectra (400–4000 cm^{-1}) were recorded from KBr pellets on a Nicolet Magna IR 750 series-II FTIR spectrophotometer. EPR spectra of polycrystalline samples were recorded using a Varian Century Series X-band EPR spectrophotometer having 100 KHz magnetic field modulation (model E 109) and equipped with a low-temperature quartz Dewar for low-temperature measurements. Room temperature magnetic susceptibilities were recorded on a PAR vibrating sample magnetometer using $Hg[Co(NCS)_4]$ as the calibrant. Diamagnetic corrections were estimated from Pascal's constants. TGA and DTA curves were recorded simultaneously on a Perkin–Elmer, Model Pyris Dimond TG/DTA in static dry nitrogen at a heating rate of 5 °C min^{-1}. Electrochemical measurements were carried out using a computer controlled PAR model 263A VERSASTAT electrochemical instrument with a glassy carbon disk (4 mm diameter, EG&G instrument) as the working electrode. All the results were collected at 25 ± 0.5 °C with reference to the Ag/AgCl electrode. All the solutions were purged with pure argon gas for at least 10 min prior to each experiment. Junction potentials were not corrected. Electronic spectra was recorded on an Agilent 8453 UV–Vis diode array spectrophotometer with a Peltier thermostatic temperature control facility at 25 ± 0.10 °C.

2.2. Syntheses

Caution! Since perchlorate salts are potentially explosive, only small amounts of the materials should be handled with care.

Preparation of $Cu(ClO_4)_2\cdot 6H_2O$, $[Cu(en)_2](ClO_4)_2$, $Na_2[Ni(CN)_4]\cdot 3H_2O$ and the starting material $[Cu(nelin)](ClO_4)_2$ (**1**) have been mentioned elsewhere [7,18] and the purity of each was checked by CHN analysis.

2.2.1. Synthesis of $[Cu(nelin)(H_2O)_2]_2[Fe(CN)_6]\cdot 6H_2O$ (*2*)

To an aqueous solution of $[Cu(nelin)](ClO_4)_2$ (0.576 g, 1.0 mmol), $K_4[Fe(CN)_6]$ (0.375 g, 1.0 mmol) dissolved in a minimum volume of water was added dropwise with constant stirring over 5 min. The precipitate that appeared initially was filtered off and the deep blue filtrate was kept in a refrigerator at 4 °C for several weeks, during which time dark brown block shaped crystals of **2** suitable for X-ray study were obtained. These were washed with cold water and dried in air at room temperature. Yield: 62% based on $[Cu(nelin)](ClO_4)_2$. *Anal.* Calc. for $C_{22}H_{62}Cu_2FeN_{16}O_{14}$: C, 27.56; H, 6.47; N, 23.39. Found: C, 27.92; H, 6.88; N, 23.06%.

IR in cm^{-1} (KBr): 3582 (s,br), 3495 (w,br), 3287 (w), 3227 (w,m), 3173 (w,sh), 2959 (w), 2886 (w), 2045 (vs), 1604 (s), 1548 (s), 1346 (s). μ_{eff} (per monomer): 1.67 μ_B at 27 °C. Electronic spectrum (water): λ_{max} = 532 nm (ε: 61.2 M^{-1} cm^{-1}).

2.2.2. Synthesis of $[\{Cu(nelin)\}_2Ni(CN)_4](ClO_4)_2\cdot 2H_2O$ (*3*)

To an aqueous solution of $[Cu(nelin)](ClO_4)_2$ (0.576 g, 1.0 mmol), $Na_2[Ni(CN)_4]\cdot 3H_2O$ (0.158 g, 0.6 mmol) dissolved in a minimum volume of water was added dropwise with constant stirring over 5 min. The precipitate that appeared initially was filtered off and the deep blue colored filtrate was allowed to undergo slow evaporation at ambient temperature in the open air. After several weeks, dark blue needle shape shiny crystals of **3** suitable for an X-ray study were obtained from the filtrate, which were filtered and washed with cold water followed by diethyl ether and dried in air at room temperature. Yield: 49%. based on $[Cu(nelin)](ClO_4)_2$. *Anal.* Calc. for $C_{20}H_{46}Cl_2Cu_2N_{14}NiO_{14}$: C, 24.91; H, 4.77; N, 20.34. Found: C, 25.01; H, 4.41; N, 20.06%.

IR in cm^{-1} (KBr): 3609 (w), 3383 (w), 3287 (w), 3225 (w), 3151 (w), 2959 (w), 2923 (w), 2893 (w), 2141 (vs), 2124 (s), 1604 (s),

1556 (s), 1444 (s), 1350 (w), 1115 (vs), 1087 (s), 1022 (s), 978 (s), 910 (vw), 711 (w), 630 (s). μ_{eff} (per monomer): 1.76 μ_B at 25 °C. Electronic spectrum (MeCN): λ_{max} = 581 nm (ε: 73.6 M^{-1} cm^{-1}).

2.3. Crystal data collection and refinement

Intensity data for **2** and **3** were collected at 293(2) K on a Siemens P4 diffractometer using graphite monochromatized Mo Kα radiation (λ = 0.71073 Å) and the ω–2θ scan mode in the range $2.44 \leqslant \theta \leqslant 26.47^{o}$ and $2.47 \leqslant \theta \leqslant 24.00^{\circ}$, respectively. The intensities were corrected for Lorentz-polarization effects and for absorption using ψ-scans. The minimum and maximum transmission factors were 0.357 and 0.596 for **2** and 0.122 and 0.142 for **3**. The structures were solved by direct methods and all non-hydrogen atoms refined anisotropically by full matrix least squares on F^2 using the SHELXTL PLUS-PC version [25,19] and hydrogen atoms were included geometrically and refined isotropically except those of water hydrogens. Other additional information concerning the data collection and refinement of the structure are compiled in Table 1.

Table 1
Crystal data and structure refinement for **2** and **3**

Complex	**2**	**3**
Molecular formula	$C_{22}H_{62}Cu_2FeN_{16}O_{14}$	$C_{20}H_{46}Cl_2Cu_2N_{14}NiO_{14}$
Formula weight	957.76	963.40
Crystal system	Monoclinic	Monoclinic
Space group	$P2_1/n$	$P2_1/n$
Unit cell dimensions		
a (Å)	9.300(2)	8.000(2)
b (Å)	15.510(3)	16.505(3)
c (Å)	14.325(3)	13.977(3)
β (°)	99.25(3)	90.98(3)
V (Å^3)	2039.4(7)	1845.3(6)
Z	4	2
μ (mm^{-1})	1.46	1.87
Reflections collected	4435	3086
Independent reflections (R_{int})	4180 (0.0202)	2866 (0.1085)
Goodness-of-fit on F^2	1.039	1.021
Final *R* indices [$I > 2\sigma(I)$]	R_1 = 0.0388	R_1 = 0.0650
	wR_2 = 0.0961	wR_2 = 0.1609
R indices (all data)	R_1 = 0.0548	R_1 = 0.1015
	wR_2 = 0.1037	wR_2 = 0.1837

2.4. PXRD data collection

Powder X-ray diffraction data were collected on a Bruker D8 Advance powder diffractometer in the Bragg-Brentano geometry using monochromatic Cu Kα1 radiation (λ = 1.5406 Å) selected with an incident beam germanium monochromator.

3. Results and discussion

Description of the structure of $[Cu(nelin)(H_2O)_2]_2[Fe^{II}(CN)_6] \cdot 6H_2O$ (**2**). Complex **2** crystallizes in the monoclinic space group $P2_1/n$. The asymmetric unit contains half of the formula unit along with three water molecules (Fig. 1). The molecular structure of complex **2** consists of two cationic $[Cu(nelin)(H_2O)_2]^{2+}$ fragments

Table 2
Selected bond distances (Å) and bond angles (°) for **2**[*] and **3**[*]

2		**3**	
Cu–N(1)	2.017(3)	Cu–N(1)	2.032(6)
Cu–N(2)	2.017(2)	Cu–N(2)	2.020(7)
Cu–N(3)	2.027(2)	Cu–N(3)	2.012(7)
Cu–N(4)	2.009(2)	Cu–N(4)	2.024(7)
Cu–OW1	2.413(2)	Cu–N(6)	2.294(6)
Cu–OW2	2.722(2)	Cu–O(1′)	2.936(15)
Fe′–C(2′)	1.927(3)	Ni–C(6)	1.870(7)
Fe′–C(3′)	1.923(3)	Ni–C(7)	1.875(8)
Fe′–C(4′)	1.917(3)	N(6)–C(6)	1.143(9)
N(2′)–C(2′)	1.161(4)	N(7)–C(7)	1.136(10)
N(5)–O(1)	1.206(4)	N(21)–O(21)	1.181(11)
N(5)–O(2)	1.223(4)	N(21)–O(22)	1.181(10)
N(2)–Cu–N(1)	85.3(1)	N(2)–Cu–N(1)	91.9(3)
N(2)–Cu–N(3)	94.0 (1)	N(2)–Cu–N(3)	85.8 (3)
N(1)–Cu–N(3)	174.2(1)	N(1)–Cu–N(3)	169.4(2)
N(2)–Cu–N(4)	177.3(1)	N(2)–Cu–N(4)	167.8(3)
N(1)–Cu–N(4)	95.1(1)	N(1)–Cu–N(4)	85.4(3)
N(3)–Cu–N(4)	85.3(9)	N(3)–Cu–N(4)	94.6(3)
N(4)–Cu–OW1	93.7(1)	N(2)–Cu–N(6)	92.9(3)
N(2)–Cu–OW1	88.9(1)	N(1)–Cu–N(6)	93.8(2)
N(1)–Cu–OW1	91.9(1)	N(3)–Cu–N(6)	96.7(3)
N(3)–Cu–OW1	93.7(1)	Ni–C(7)–N(7)	176.9(7)
OW1–Cu–OW2	174.6(6)	Ni–C(6)–N(6)	176.2(7)
Fe′–C(2′)–N(2′)	179.1(3)	C(6)–Ni–C(6)#2	180.0(6)
C(2′)–Fe′–C(2′)#1	180.0(5)	C(7)–Ni–C(7)#2	180.0(5)

[*] Symmetry transformation used to generate equivalent atoms: #1 $-x$, $-y$, $-z$; #2 $-x+1$, $-y$, $-z$.

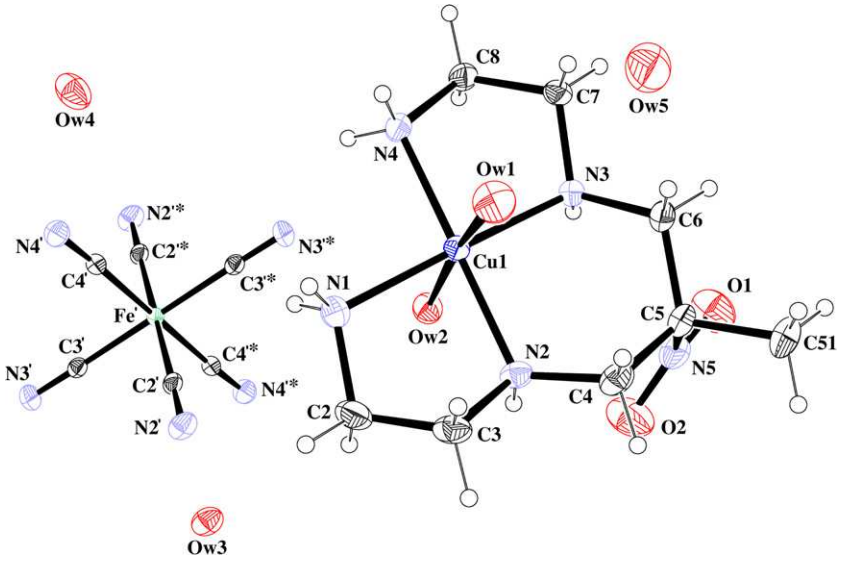

Fig. 1. ORTEP diagram (30% ellipsoidal probability) with the atom numbering scheme for complex **2** ([*] = $-x+1$, $-y$, $-z$).

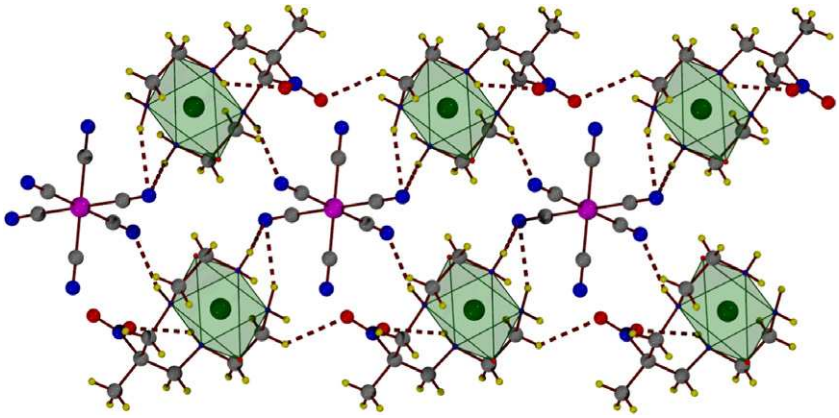

Fig. 2. H-bonded supramolecular 1D chain of anions and cations for complex **2** along the *a*-axis.

the charges of which are counter-balanced by the $[Fe^{II}(CN)_6]^{4-}$ anion along with six water molecules. The coordination geometry of each copper(II) atom is best described as distorted octahedral. The square plane is constructed by the four nitrogen atoms (N1, N2, N3 and N4) of the diaza-diamine ligand and the axial sites are occupied by two more distant oxygen atoms of two water molecules. The N(4)–Cu–N(2) (177.3(1)°) and N(1)–Cu–N(3) (174.2(1)°) angles in the equatorial plane slightly deviate from 180° and the average of the four OW_1–Cu–N angles (92.1°) (Table 2) is slightly higher than 90°. All these indicate a slight distortion from a regular octahedral geometry with the copper center situated at 0.100(4) Å above the mean plane towards the axial OW1 water molecule. In the equatorial plane, the Cu–N bond distances vary from 2.009(2) to 2.027(2) Å (avg. 2.017(2) Å) and are comparable with the previously reported values [18]. It is noteworthy that the two axial Cu–OW bond distances are not identical; Cu–OW_1 2.413(2) and Cu–OW_2 2.722(2) Å; probably due to a different extent of H-bonding. On the other hand, $[Fe^{II}(CN)_6]^{4-}$ retains its perfect octahedral geometry (Table 2).

Hydrogen bonds play a pivotal role in assembling the discrete cationic and anionic entities towards higher dimensionality. The packing diagram clearly indicates that all the ferrocyanide ions occupy special positions and the participation of the cyano nitrogen in extensive intermolecular H-bonding. The $[Fe(CN)_6]^{4-}$ unit act as a template for the organization of four $[Cu(nelin)]^{2+}$ units around it and due to successive hydrogen bonding this gives rise to a supramolecular chain along the crystallographic *a*-axis (Fig. 2, Table 3). The H-bonded polymeric chains are three dimensionally interlinked through hydrogen bonding (N4–H44···O2) to form irregular honeycomb-like channels (Fig. 3), which accommodate a one dimensional helical water chain as shown in Fig. 4. Three lattice water molecules (OW3, OW4, OW5), by hydrogen bonding association with themselves together with the coordinated water molecule (OW1), give rise to this helical assembly. The hydrogen bonding distances are OW1···OW3 = 2.818(4) Å; OW3···OW4 = 2.889(4) Å; OW4···OW5 = 2.807(4) Å; OW5···OW1 = 2.724(4) Å. The pitch of the helical water chain is 9.3 Å and it is supported within the channel by three more hydrogen bonding contacts OW3···OW2 = 2.804(4) Å; OW3···N2′ = 2.729(4) Å and OW3···N4′ = 2.887(4) with the wall as it propagates along the *a*-axis. Each of the channels is symmetric and it is divided

Table 3
Important H-bonding parameters for **2** and **3**

D–H···A	D–H (Å)	H···A (Å)	D–A (Å)	∠D–H···A (°)	Symmetry[a]
Complex ***2***					
N2–H2···O2	0.910	2.230	2.835(4)	123.0	
N3–H3···N5	0.910	2.620	2.947(4)	102.0	
N3–H3···N3′	0.910	2.350	3.222(4)	161.0	2a
N1–H12···N4′	0.900	2.450	3.279(4)	154.0	2b
N4–H43···N4′	0.900	2.610	3.410(4)	149.0	2b
N4–H44···O2	0.900	2.380	3.128(4)	140.0	2c
Complex ***3***					
N1–H1···O3′	0.910	2.200	3.061(14)	157.0	
N2–H1···O3′	0.910	2.250	3.078(14)	151.0	
N2–H1···O21	0.910	2.490	3.032(13)	119.0	
N2–H31···N7	0.900	2.200	3.091(10)	171.0	3a
N3–H32···O2′	0.900	2.350	3.057(14)	135.0	3b
N4–H41···O4′	0.900	2.560	3.304(17)	141.0	3c
N4–H42···N7	0.900	2.620	3.441(10)	151.0	3a

[a] 2a: 1/2 + *x*, 1/2 − *y*, 1/2 + *z*; 2b: 1/2 − *x*, 1/2 + *y*, 1/2 − *z*; 2c: 1/2 + *x*, 3/2 − *y*, 1/2 + *z*. 3a: 1/2 − *x*, 1/2 + *y*, 1/2 − *z*; 3b: 1/2 + *x*, 1/2 − *y*, −1/2 + *z*; 3c: 1 + *x*, *y*, *z*.

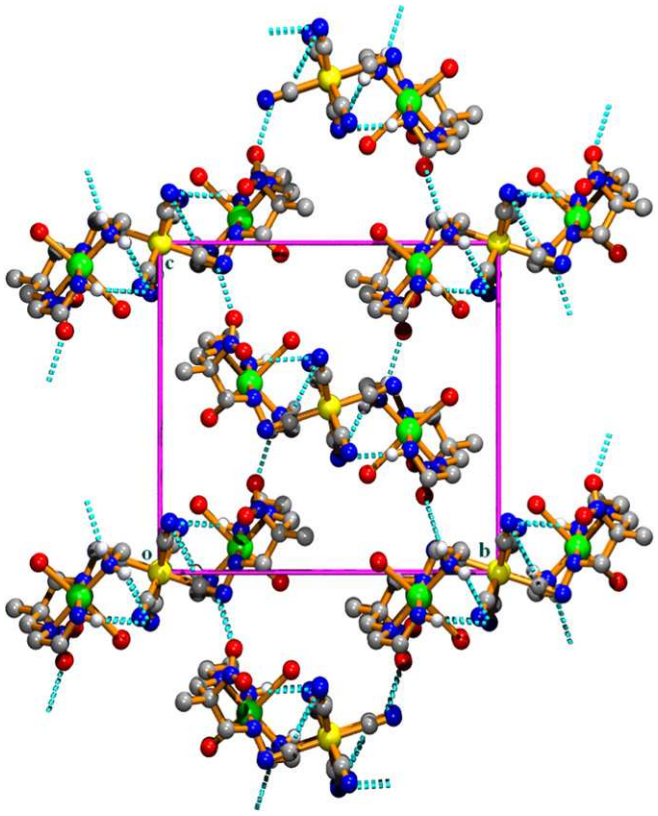

Fig. 3. Formation of supramolecular channels along the *a*-axis through interlinking of nearby chains for complex **2**.

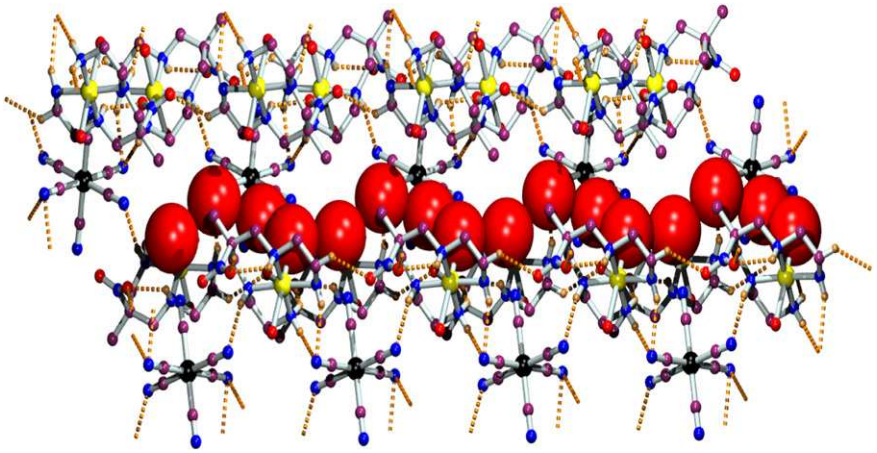

Fig. 4. Helical water chain comprising of three lattice water molecules and one coordinated water molecule (OW1) within one half of the channel for complex **2**.

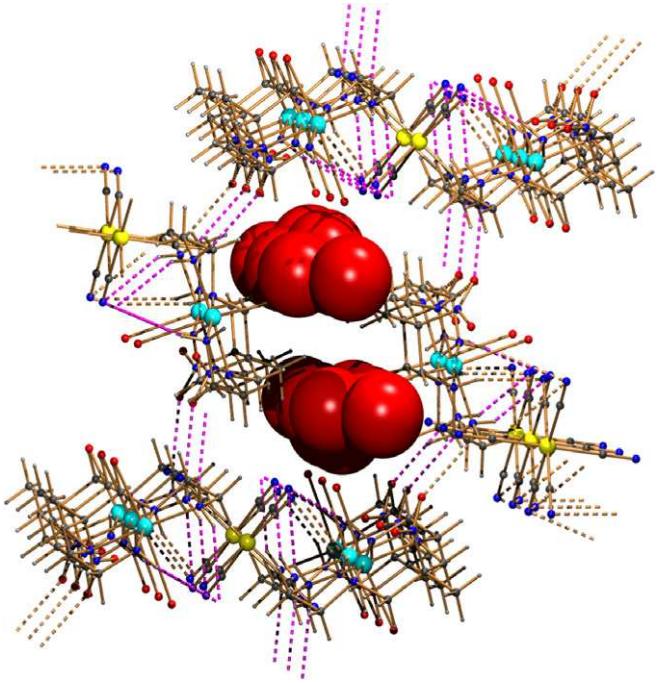

Fig. 5. The symmetric channels accommodate helical water chains in either half. Helical water chains in either half run in opposite directions to each other for complex **2**.

into two halves. Each half accomodates a helical water chain which run in opposite directions to each other (Fig. 5).

3.1. Description of structure of $[\{Cu(nelin)\}_2Ni(CN)_4](ClO_4)_2.2H_2O$ (3)

The molecular structure of **3** consists of a trinuclear $[\{Cu(nelin)\}_2Ni(CN)_4]^{2+}$ cation, two perchlorate anions and two water molecules (Fig. 6). The asymmetric unit consists of one half of the formula unit with the inversion center located at the nickel atom. The $[Ni(CN)_4]^{2-}$ anion is coordinated to two $[Cu(nelin)]^{2+}$ cations through two cyano groups bridging in a di-*trans* fashion, leaving the two other *trans*-CN groups uncoordinated, and complex **3** in this sense is comparable to $[Cu(HL)]_2[Ni(CN)_4]\cdot 4H_2O$ [7b] (H_2L = 3,9-dimethyl-4,8-diazaundec-3,8-diene-2,10-dione-dioxime). The bonding arrangement of this trinuclear unit is shown in Fig. 6 and selected bond distances and angles are given in Table 2.

The coordination geometry around the copper center is best described by a square pyramid with the geometrical factor $\tau = 0.03$ [7a]. The basal plane is constructed by the four nitrogen atoms of the diaza-diamine ligand and the apical position is occupied by the nitrogen atom of the bridging cyanide. In the basal plane the Cu–N bond distances vary from 2.012(7) to 2.032(6) Å, whilst that of the apical Cu–N(6) is 2.294(6) Å, which is significantly longer than the basal Cu–N bond lengths. The N(1)–Cu–N(3), 169.4(2)° and N(2)–Cu–N(4), 167.8(3)° angles in the basal plane deviate significantly from 180° and the four N(6)–Cu–N(x) [x = 1, 2, 3 and 4] angles are larger than 90° (avg. 95.6(3)°), indicating that the coordination geometry around each copper(II) center is a distorted square pyramid. The copper center is situated 0.199 Å above the plane towards the apical direction. It is interesting to mention here that one oxygen atom from the perchlorate anion, O(1′), is at an elongated contact distance 2.936(15) Å to the copper(II) center. The bridging cyanide coordinates to the copper ion in a bent fashion with a C(6)–N(6)–Cu bond angle of 165.3(6)°. The intramolecular Cu···Cu separation is 10.497 Å. Like the earlier trends [7b] no significant difference has been observed here between the bridging (C(6)–N(6) = 1.143(9) Å) and terminal (C(7)–N(7) = 1.136(10) Å) cyano groups and $[Ni(CN)_4]^{2-}$ retains its square planer(SP) geometry (Table 2).

As shown in Fig. 7, the trinuclear units are arranged in successive rows in a herringbone fashion and the bifurcated hydrogen bonding (N3–H31···N7 and N4–H42···N7) (Table 3) through the uncoordinated terminals of the $[Ni(CN)_4]^{2-}$ units give rise to a supramolecular (4,4) network in the (202) plane. In this arrangement the $[Ni(CN)_4]^{2-}$ units act as a template for a (4,4) net architecture. Perchlorate anions and lattice water molecules occupy the void spaces within this network and bind to the cationic part of the trinuclear units through hydrogen bonding (Table 3). Successive (202) planes are stacked along the [101] direction through C–H···O hydrogen bonding (Fig. 8).

3.2. IR study

The positions of the relevant IR bands of complexes **2** and **3** are given in Section 2. The IR active bands fall in the region of *ca.* 3151–3600 cm^{-1} for both complexes which is characteristic for ν(O–H) and ν(N–H) groups. For cyano complexes, absorption bands due to ν_{CN} stretching vibrations are very characteristic. In $K_4[Fe^{II}(CN)_6]$ the ν_{CN} band appears at 2042 cm^{-1} [20] and in complex **2** a sharp peak at *ca.* 2045 cm^{-1} clearly indicates that all the cyano groups of the ferrocyanide ion are terminal. For the tetracyanonickelate anion this absorption band appears at 2128 cm^{-1} [20]. On bridging

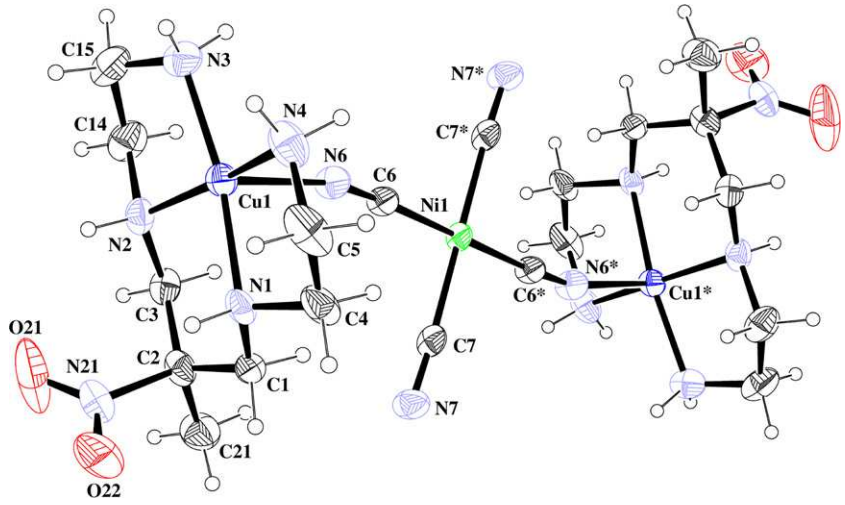

Fig. 6. ORTEP view (30% ellipsoidal probability) of the trinuclear unit of **3** with the atom numbering scheme. Perchlorate ions and water molecules are omitted for clarity (* = $-x$, $-y$, $-z$).

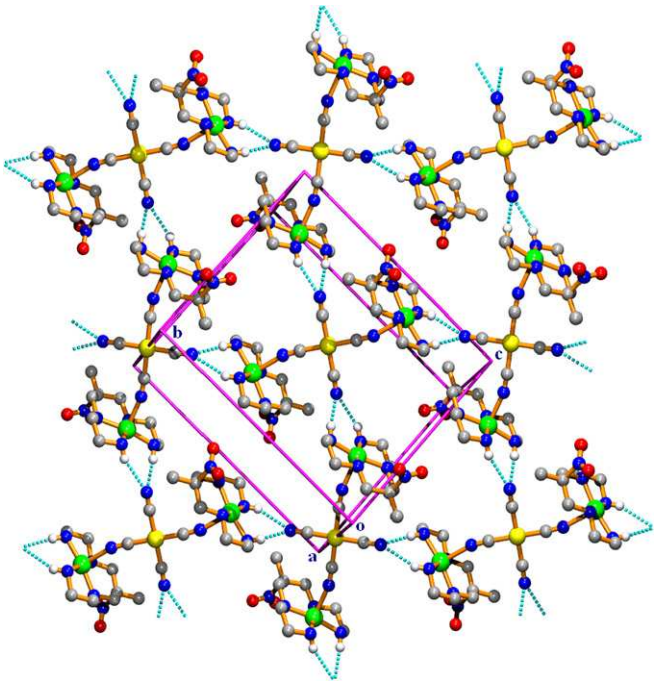

Fig. 7. The (4,4) supramolecular network in the (202) plane of complex **3**. $[Ni(CN)_4]^{2-}$ units act as a template for this network. Perchlorate ions and water molecules, which are omitted for clarity, occupy the void space within the network.

via N atoms this band shifts to a higher wave number. The two ν_{CN} IR bands appearing at 2124 (vs) and 2141 (s) cm^{-1} for **3** can be assigned to the terminal and bridging cyanide groups, respectively [20a]. The characteristic IR bands corresponding to the nitro group appear for **2** at 1548 cm^{-1} (s, ν_{as}) and 1346 cm^{-1} (m, ν_s) and that for **3** at 1556 cm^{-1} (s, ν_{as}) and 1350 cm^{-1} (w, ν_s) [1g]. Additionally, a strong band near 1115 cm^{-1} and a sharp band near 623 cm^{-1} indicate the presence of an uncoordinated perchlorate anion for complex **3** [20b]. All other bands appear at their usual positions.

3.3. Thermal analyses

Complex **2** remains unchanged at room temperature (27 °C) for an indefinite period. TGA studies show that total water loss occurs in two narrow temperature regions: an 8.57% weight loss was observed in between 40 and 90 °C, which is almost equivalent to a loss of 4.5 water molecules. This is accompanied by a small *endo*-effect on the DTA curve at *ca.* 80 °C. Obviously these are due to non-coordinated lattice water molecules present in the cavities. On gradual heating a further 8.51% weight loss was monitored in between 100 and 130 °C and the total weight loss is equivalent to 4.46 water molecules. These are partially lattice as well as coordinated water molecules. The corresponding endo-therm was observed at *ca.* 122 °C. The remaining water molecules are retained up to 140 °C, after which the complex undergoes an immediate decomposition with a large exothermal peak at *ca.* 145 °C in the DTA curve. Losses of water molecules in different stages are due to the different extent of H-bonding. For example, some water mol-

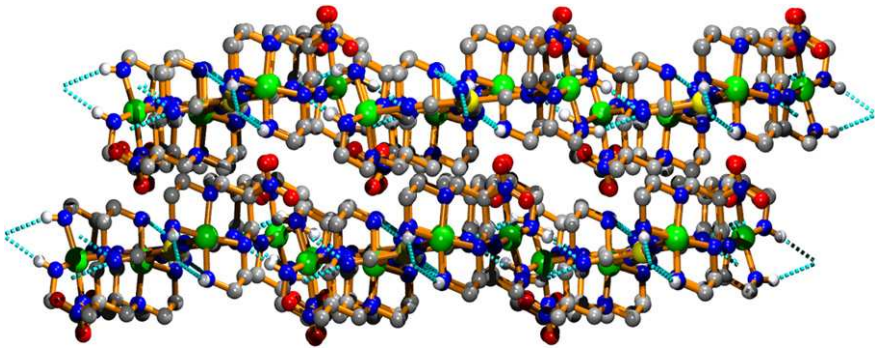

Fig. 8. The disposition of successive (202) layers in complex **3**.

ecules are doubly H-bonded with two neighbouring water molecules while some water molecules are triply H-bonded with an additional H-bond to a cyano nitrogen atom. As it is envisaged that the network is purely built up of strong H-bonding, complete removal of all the water molecules ultimately results in collapse of the structural morphology. This is evident from the powder X-ray diffraction (PXRD) pattern (Fig. 9).

Thermal decomposition of complex **3** starts at *ca.* 65 °C and consequently the complex eliminates its two uncoordinated water molecules, and the process continues up to *ca.* 100 °C (found/calc.: 3.70%/3.74% with respect to loss of weight%). This is accompanied by a small *endo*-effect on the DTA curve at *ca.* 90 °C. The anhydrous complex, having the formula $[\{Cu(nelin)\}_2Ni(CN)_4](ClO_4)_2$, maintains its thermal stability up to *ca.* 180 °C. After that the complex undergoes an immediate decomposition with a small exothermal peak at *ca.* 190 °C in the DTA curve. Since the complex contains the perchlorate anion, we have not carried out the experiment beyond 200 °C.

3.4. PXRD analysis

To study the effect of dehydration on the structure, a PXRD pattern of complex **2** was recorded at 27 °C (Fig. 9a). It was then heated to (130 ± 2) °C in a stream of nitrogen and was kept at this temperature for 30 min. An X-ray powder diffraction pattern (Fig. 9b) was recorded almost immediately on cooling the compound to room temperature (27 °C), which showed marked changes in the diffraction pattern compare to that of the original phase (Fig. 9a). The PXRD pattern of the dehydrated species clearly indicates that in addition to water removal from the original crystalline structure, it has transformed into a quasi glassy material. Dehydration of the hydrated species to generate a glassy state is most unusual, since up until now only hydrated trehalose [21], raffinose [22] and magnesium acetate [23] have been reported to have this property. Such a finding may be explored by crystal engineers in a more applied way.

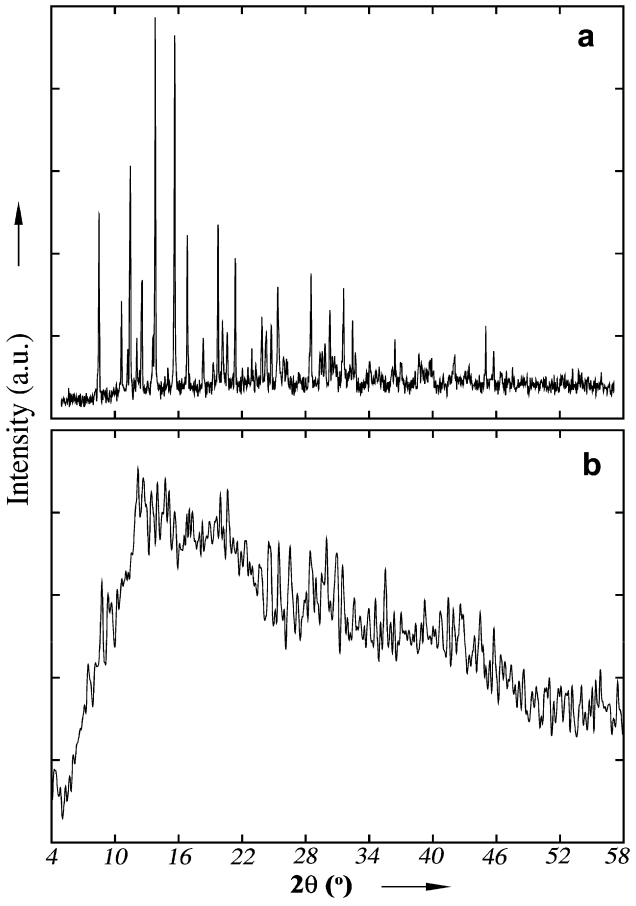

Fig. 9. (a) PXRD pattern (complex **2**); (b) PXRD patten (complex **2** after heating).

3.5. EPR studies

Room temperature solid state EPR of a polycrystalline sample of **2** is typical for a mononuclear copper(II) complex with axial distortion, and the elongation of the axis is characterized by $g_{||} = 2.21$ and $g_{\perp} = 2.01$. An almost identical spectrum for **3** is characterized by $g_{||} = 2.11$ and $g_{\perp} = 2.04$. The observed values ($g_{||} > g_{\perp}$) confirm that the unpaired electron resides in the $d_{x^2-y^2}$ orbital. In the water–alcohol glass phase at 77 K complex 2 exhibits a typical four-line hyperfine spectra with $g_{||} = 2.11$, $g_{\perp} = 2.02$, $A_{||} = 150$ Oe and $A_{\perp} = 5$ Oe at $V = 9.45$ MHz. On standing the solution for 2–5 days a moderately strong signal at $g = 4.3$ indicates the presence of Fe^{III} species in the system [24]. This may be attributed to the oxidation of a portion of $[Fe^{II}(CN)_6]^{4-}$ to $[Fe^{III}(CN)_6]^{3-}$ in aqueous solution, as indicated by the slow disappearance of the color of the complex with time.

3.6. Electrochemical studies

The electrochemical properties of the complexes $[Cu(nelin)(H_2O)_2]_2[Fe^{II}(CN)_6]\cdot 6H_2O$ (**2**) and $[\{Cu(nelin)\}_2Ni(CN)_4](ClO_4)_2\cdot 2H_2O$ (**3**) were investigated using the cyclic voltammetric technique in aqueous and in MeCN solutions, respectively, with Ag/AgCl as the reference electrode. The cyclic voltammetric behavior of the parent complex $[Cu(nelin)](ClO_4)_2$ (**1**) was also studied under similar conditions in aqueous and in MeCN media to compare the results. All the electrochemical data are summarized in Table 4.

The electrochemical responses of complex **1** in aqueous solution were found to be highly influenced by the scan rate. At a scan rate of $\sim$1.0 V s^{-1}, a single irreversible reduction peak at a potential of *ca.* −0.94 V was found and attributed to a four-electron reduction process (Eq. (1)), as generally observed for nitro compounds in protic solvents [15,16]:

$$-NO_2 + 4H^+ + 4e^- \rightarrow -NHOH + H_2O \quad (1)$$

At appreciably lower scan rates, the situation is quite different. Thus, at a scan rate of 0.05 V s^{-1}, two irreversible reduction waves having peaks *viz.* A and B at potentials of *ca.* −0.69 V and −1.0 V, respectively, were observed, and on the reverse sweep an anodic peak (D) at *ca.* −0.31 V was monitored. After a second sweep, another reduction peak C at *ca.* −0.49 V in addition to peaks A and B appeared, while the anodic peak D remained invariant with respect to its position (Fig. 10). However, it is important to note that after the first sweep the peak intensities for A and B were greatly diminished while that of D remained almost unchanged. In order to assess the number of electron transfers involved in these processes, peak A was assigned to be a one-electron reduction of a nitro group to a nitro-radical anion followed by a three-electron reduction of the nitro-radical anion (peak B) to the hydroxylamine derivative (Scheme 1). These are comparable with the nitro-containing heterocyclic drug metronidazole [17].

Surprisingly, no cathodic wave (peak C), for a $Cu^{II} \rightarrow Cu^{I}$ reduction was observed during the first scan. However, if we assume that the anodic oxidation peak D observed in the reverse sweep in the first scan is due to oxidation of $Cu^{I} \rightarrow Cu^{II}$, then it is likely to assume that the nitro-radical anion generated in the first sweep is responsible for initiation of the reduction of the Cu^{II} center, which in the reverse sweep undergoes oxidation. Thus keeping

Table 4
Electrochemical parameters[a]

Complex (1.0×10^{-3} M)	Solvent	Supporting electrolyte (0.1 M)	E_{pc} (V)	E_{pa} (V)	ΔE_p (V)	$E_{1/2}$ (V)	Redox couple and reaction
$[Cu(nelin)](ClO_4)_2$ **(1)**	Water	$NaClO_4$	−1.06				$-NO_2 \rightarrow -NHOH$[b]
(Reported)	pH ~ 6				0.08	−0.59	Cu^{II}/Cu^{I}[b]
$[Cu(nelin)](ClO_4)_2$ (**1**) (Our Investigation)	Water	$NaClO_4$	−0.69				$-NO_2 \rightarrow NO_2^-$
			−1.05				$-NO_2^- \rightarrow -NHOH$
	pH 6.4		−0.49	−0.31	0.18	−0.40	Cu^{II}/Cu^{I}
	MeCN	TBAP	−0.96				Cu^{I}/Cu^{0}
			−1.65				$-NO_2 \rightarrow NO_2^-$
			−0.62	−0.36	0.26	−0.49	Cu^{II}/Cu^{I}
$[Cu(nelin)(H_2O)_2]_2$. $[Fe(CN)_6].6H_2O$ (**2**)	Water pH 6.8	$NaClO_4$	−0.64				$-NO_2 \rightarrow NO_2^-$
			−0.87				$-NO_2^- \rightarrow -NHOH$
			0.22	0.40	0.18	0.31	Fe^{III}/Fe^{II}
$[\{Cu(nelin)\}_2Ni(CN)_4](ClO_4)_2 \cdot 2H_2O$ **(3)**	MeCN	TBAP	−0.99				Cu^{I}/Cu^{0}
			−1.63				$-NO_2 \rightarrow -NO_2^-$
			−0.58	−0.32	0.26	−0.45	Cu^{II}/Cu^{I}
Ferrocene	MeCN	TBAP	0.36	0.52	0.16	0.44	Fe^{III}/Fe^{II}

[a] Maximum error ±5%; all potentials are measured against the Ag/AgCl reference electrode; $E_{1/2}$ is determined as 1/2 ($E_{pc} + E_{pa}$).
[b] Reported values (Ref. [15]): measured for DME *vs.* Ag/Ag^+.

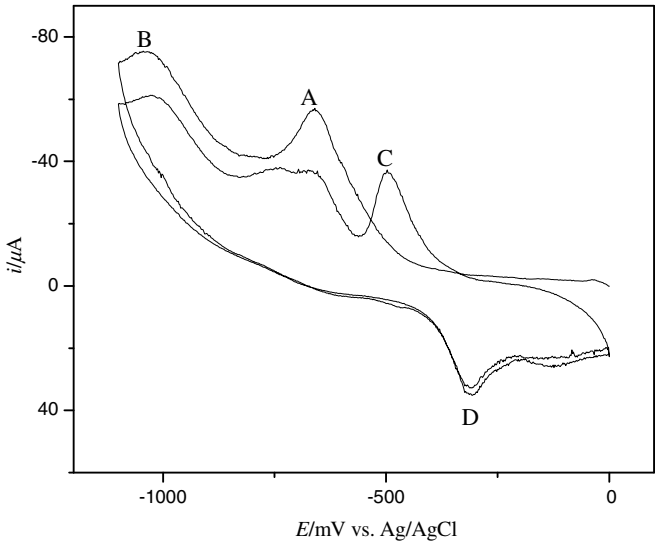

Fig. 10. Two successive cyclic voltammograms of **1** in water at a scan rate of 0.05 V s^{-1}.

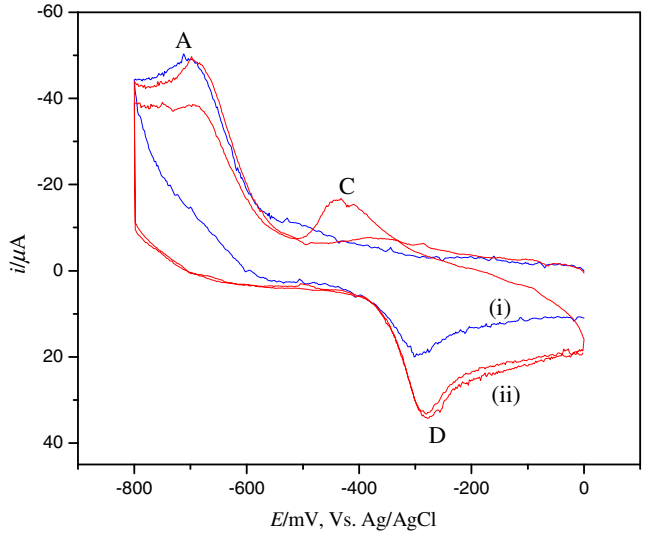

Fig. 11. Comparative cyclic voltammograms of **1** in water at a scan rate of 0.05 V s^{-1}: (i) The sweep is reversed just after formation of the nitro-radical anion (A), (ii) the sweep is reversed just after formation of the nitro-radical anion (A) but is delayed for 5 min.

$$Cu^{II}R - NO_2 + e^- \rightarrow Cu^{II}R - NO_2^{\cdot -} \qquad (2)$$

$$Cu^{II}R - NO_2^{\cdot -} + 3e^- + 4H^+ \rightarrow Cu^{II}R\text{-}NHOH + H_2O \qquad (3)$$

Scheme 1.

the copper(II) to copper(I) reduction silent in the first scan and its appearance from the second scan (peak C) may be thought of that the original Cu^{II} complex remains silent towards the redox transformation. The above proposition is supported by the following observations:

(1) When the scan was reversed just before the generation of the nitro-radical anion (peak A), the anodic peak D was absent.
(2) When the scan was reversed just after the appearance of peak A, the anodic peak D was observed.
(3) If the scan is reversed just after the appearance of peak A and is delayed for 5 min at the same potential the intensity of the anodic peak (D) is increased (Fig. 11).

Thus the copper(II) center in complex **1** is found to be silent towards redox transformation in the experimental scan rate at the first scan. Now the question arises, why is the copper(II) center in **1** silent towards this redox process. A reasonable argument can be made as follows: the copper(II) center is deeply buried in the ligand environment while the NO_2 group on the ligand fragment is well exposed in space for redox processes. Thus, it is the NO_2 group which first undergoes reduction to give the nitro-radical anion $Cu^{II}RNO_2^-$. The highly reactive nitro-radical anion thus generated electrochemically from the nitro group, in close proximity towards the metal center due to conformational puckering, [15] immediately transmits its electron to facilitate the copper(II) reduction to copper(I), which concomitantly undergoes some kind of structural modification to give $Cu^{I}R^{*}NO_2$. This modified species, only after oxidation to $Cu^{II}R^{*}NO_2$, can initiate its second time reduction without the assistance from a nitro-radical anion; and by this way $E_{1/2}$ for Cu^{II}/Cu^{I} was estimated as −0.40 V. All these transformations are given in Scheme 2.

Considering the overall cyclic voltammetric pattern of **1** in aqueous solution in the above mentioned slow scan rate, a

$$Cu^{II}(R\text{-}NO_2)^{+} \xrightarrow{e^-} Cu^{II}(R\text{-}NO_2^{\bullet -}) \xrightarrow{iet} Cu^{I}(R\text{-}NO_2) \xrightarrow{cm} Cu^{I}(R^{*}\text{-}NO_2)$$

$$\xrightarrow{-e^-} Cu^{II}(R^{*-}NO_2) \longrightarrow Cu^{I}(R^{*}\text{-}NO_2)$$

iet = intramolecular electron transfer; cm = conformational modification

Scheme 2.

speculative explanation may be furnished: peak A is just due to the irreversible reduction of $[Cu^{II}(nelin)]^{2+}$ to $[Cu^{I}(nelin)]^{+}$; which subsequently undergoes decomposition to generate the free Cu^{+} ion, which in turn is reoxidized to the Cu^{2+} ion (peak D) and re-reduced to the bare Cu^{+} ion (peak C). However, a serious problem for such a proposition arises from the $E_{1/2}$ value for the Cu^{II}/Cu^{I} couple (−0.40 V *versus* Ag/AgCl). The observed potential (−0.18 V *versus* NHE) is much more negative than the corresponding standard electrode potential for the free Cu^{II}/Cu^{I} couple (0.15 V). Moreover, the free Cu^{+} ion is too susceptible for disproportionation in aqueous solution, but no such indication was observed in the back scan, either through the appearance of an anodic stripping peak or through elemental copper deposition in the experimental solution during and after the completion of the cyclic voltammetric process. Thus the speculation of the transformation of $[Cu^{I}(nelin)]^{+}$ to $[Cu^{0}$-$(nelin)]^{0}$, or put in a better way Cu^{0}, (peak B) can be discarded safely.

The electrochemical behavior of complex **1** at the same scan rate (0.05 V s^{-1}) in MeCN (Fig. 12) was completely different from that which was observed in aqueous solution. Here, from the beginning a cathodic peak (E) for $Cu^{II} \rightarrow Cu^{I}$ reduction was observed at a potential of *ca.* −0.62 V; for which the reverse scan showed an anodic wave (H) at *ca.* −0.36 V and the corresponding $E_{1/2}$ was estimated as −0.49 V *versus* Ag/AgCl. It is important to note that after formation of the Cu^{I} complex (peak E), it subsequently undergoes slow disproportionation to Cu^{II} and Cu^{0}, and a well defined anodic stripping peak at *ca.* −0.16 V was observed for Cu^{0}. As a consequence the anodic peak (peak H) for oxidation of $Cu^{I} \rightarrow Cu^{II}$ was greatly diminished. To support this proposition two separate CV profiles were recorded, inverting the scan immediately after traversing peak E and peak F, respectively, under same scan rate (0.05 V s^{-1}). The great increment of the anodic stripping peak after traversing peak F compare to peak E, not only certified the disproportionation of the $[Cu^{I}(nelin)]^{+}$ complex but simultaneously helped to assign peak F as $Cu^{I} \rightarrow Cu^{0}$. At a comparatively higher scan rate (0.8 V s^{-1}) no such anodic stripping peak in the back scan after traversing peak E indicates the slower nature of the disproportionation reaction. Here peak G is conceivably assign to the irreversible $NO_2/-NO_2^{-}$ reduction. The cathodical fluctuation of the nitro-radical anion peak from solvent to solvent is a common feature for nitro-containing compounds [25].

In conclusion, it is clear that the nitro-radical induced reduction of $[Cu^{II}(nelin)]^{2+}$ and the reluctancy of the disproportionation reaction of the modified $Cu^{I}R^{*}NO_2$ is the main feature in aqueous medium, while the normal reduction (without any assistance of a nitro group) of $[Cu^{II}(nelin)]^{2+}$ to $[Cu^{I}(nelin)]^{+}$ followed by slow disproportionation to Cu^{II} and Cu^{0} are the mentionable characteristics in MeCN for complex 1. It also further indicates that the initial environment of $[Cu^{II}(nelin)]^{2+}$ in aqueous and in MeCN solution are to some extent different.

The electrochemical behavior of complex **2** was monitored at a slow scan rate (0.05 V s^{-1}) in aqueous medium (Fig. 13). A well defined anodic wave at *ca.* 0.40 V and a corresponding cathodic wave at *ca.* 0.22 V appeared. It was assigned to the $[Fe^{III}(CN)_6]^{3-}/[Fe^{II}(CN)_6]^{4-}$ couple and the corresponding $E_{1/2}$ was estimated as 0.31 V *versus* Ag/AgCl. From the peak height and intensity it is evident that the concentration of iron(II) is higher than that of the iron(III) species. When the scan was continued further to negative potential, two irreversible reduction peaks at potentials of *ca.* −0.72 V and −0.95 V were observed, and these are assigned to the corresponding nitro group reduction (*vide infra*). It is surprising that no Cu^{II}/Cu^{I} couple was observed even after a second sweep, as compared to that observed in the parent complex **1**. On the

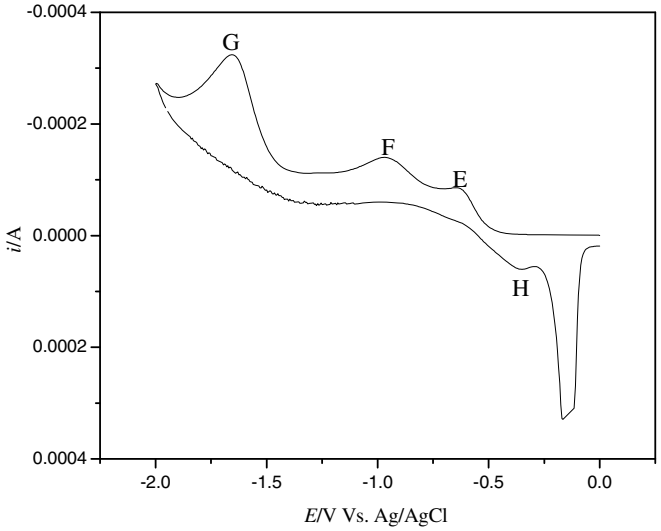

Fig. 12. Cyclic voltammogram of **1** in MeCN at a scan rate of 0.05 V s^{-1}.

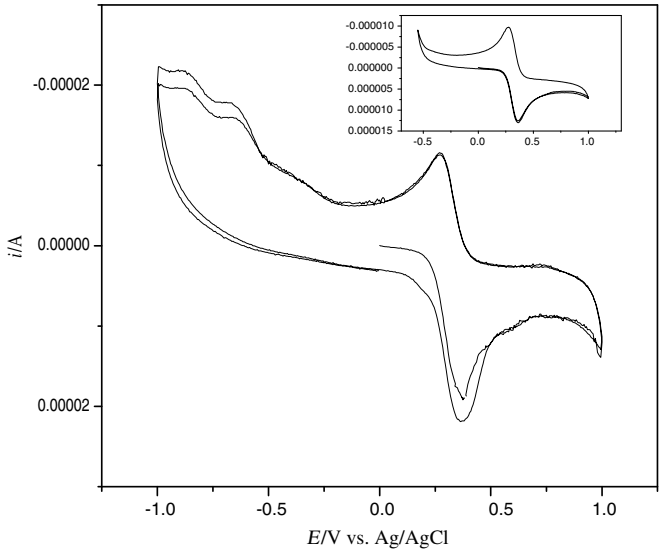

Fig. 13. Cyclic voltammograms of **2** in water at a scan rate of 0.05 V s^{-1}. The scan is reversed before nitro-radical anion formation (inset).

other hand, on the reverse sweep, the peak height of the anodic wave was markedly enhanced in comparison to that of the cathodic wave in the positive potential range, indicating the conversion of $Fe^{II} \rightarrow Fe^{III}$ increases after the nitro group reduction. Since the reduction potential of the $[Fe^{III}(CN)_6]^{3-}/[Fe^{II}(CN)_6]^{4-}$ couple is much more than that of Cu^{II}/Cu^{I} (−0.40 V *versus* Ag/AgCl for complex **1**), most probably the nitro-radical anion transfers its electron to the Fe^{III} instead of the Cu^{II} center and that is why nitro-radical induced copper(II) reduction does not take place as observed in complex **1**. Consequently the Cu^{II}/Cu^{I} couple remains silent towards redox transformation. To check whether the nitro group has any influence upon the iron center, a number of CV profiles were recorded starting from 0.0 V to 1.0 V, 1.0 V to −0.60 V (*i.e.* before nitro-radical anion generation) (Fig. 13, inset) under the same scan rate and it was observed that the peak height and intensity for the anodic and cathodic waves responsible for the $[Fe^{III}(CN)_6]^{3-}/[Fe^{II}(CN)_6]^{4-}$ couple remain invariant even after a second successive sweep. It is well known [25] that the nitro-radical anion is not generated particularly with a platinum working electrode. To confirm whether the reduction peaks arise due to nitro group reduction or for copper (II) reduction, a cathodic CV profile starting from 0.0 V to −1.2 V was recorded using platinum working electrode under same scan rate, but no peak responsible for the nitro-radical anion was observed. In conclusion, it may be assumed that only a portion of the ferrocyanide ion may coordinate to the copper(II) center, facilitating a lower energy pathway for electron transfer. This chemically generated ferricyanide ion on electrochemical processing is reduced to the ferrocyanide by capturing the electron from the nitro-radical anion. In cyclic voltammetry, such a coordinated ferrocyanide ion reduced by a generated nitro-radical, as well as the non-coordinated ferrocyanide ion, enhances the peak height for the $Fe^{II} \rightarrow Fe^{III}$ conversion in the reverse sweep.

The electrochemical behavior of complex **3** warrants special features in comparison to that of the parent complex **1** in MeCN (Fig. 14). The quasi-reversible reduction process for $Cu^{II} \rightarrow Cu^{I}$ (peak I/L) appeared at a slightly more positive potential than that in complex **1** under similar conditions and the corresponding $E_{1/2}$ was estimated as −0.45 V *versus* Ag/AgCl. It is noteworthy that compared to complex **1**, both electrochemical reduction and oxidation for the Cu^{II}/Cu^{I} couple in complex **3** are more facile and this is attributed to the axial ligation of $[Ni(CN)_4]^{2-}$ to the $[Cu(nelin)]^{2+}$ precursor [7b]. Another interesting aspect of complex **3** compared to **1** is that after formation of the Cu^{I} complex (peak I) it does not undergo any disproportionation reaction like 1 at either high or slow scan rates. This is also due to the axial attachment of $[Ni(CN)_4]^{2-}$ to the $[Cu^{II}(nelin)]^{+2}$ moiety which ultimately stabilizes the $[Cu^{I}(nelin)]^{+}$ species. No anodic stripping peak was observed during the back scan after traversing from peak I. Peak J is certainly for $[Cu^{0}(nelin)]^{0}$, or put in better way Cu^{0}, which on back scanning produces an anodic stripping peak at *ca.* 0.0 V.

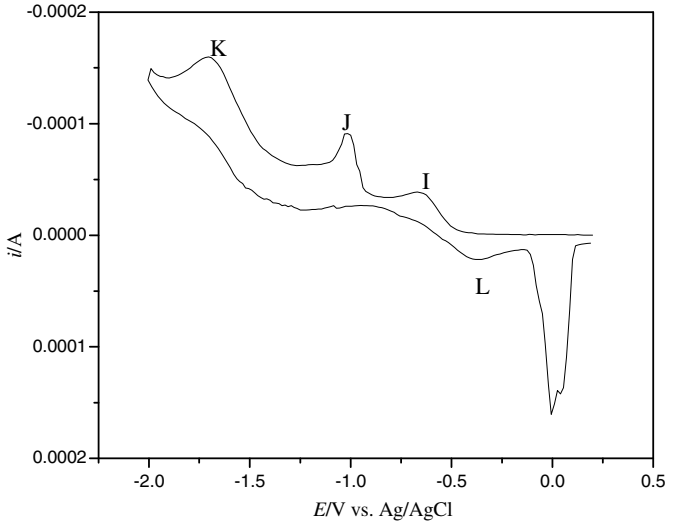

Fig. 14. Cyclic voltammogram of **3** in MeCN at a scan rate of 0.05 V s^{-1}.

4. Conclusions

Two new complexes, $[Cu(nelin)(H_2O)_2]_2[Fe(CN)_6] \cdot 6H_2O$ (**2**) and $[\{Cu(nelin)\}_2Ni(CN)_4](ClO_4)_2 \cdot 2H_2O$ (**3**), have been synthesized using a nitroalkyl-substituted $Cu^{II}N_4$ precursor and have been characterized using the single crystal X-ray diffraction technique. The H-bonded 1D chains of 2 along the *a*-axis, generated from supramolecular synthons using cations and anions, are further propagated into a 3D array to form irregular honeycomb-like channels which are divided into two halves, in each half there is a helical water chain which runs in opposite directions to each other. In complex **3** trinuclear units are arranged in successive rows in a herringbone fashion and bifurcated hydrogen bonding through the uncoordinated terminals of the $[Ni(CN)_4]^{2-}$ units give rise to a supramolecular (4,4) network. Complex **2** exhibits a quasi-glass nature on dehydration, which is important in material science. The electrochemical properties of **1**, 2 and **3** have been investigated in comparative ways using the cyclic voltammetric technique in aqueous and in MeCN solutions with Ag/AgCl as the reference electrode. Electrochemical studies in aqueous medium generate the one-electron reduced nitro-radical anion which is highly important and may find application as a radio-sensitized drug in cancer treatment. Although organic, especially aromatic, nitro compounds have widespread application in medicine and cancer therapy, there is direct proof that nitro-radical anions are involved as an obligate intermediate but in many cases they act as a direct damaging toxin. The corresponding use of coordination complexes bearing a nitro group on a side arm of a ligand fragment has not yet been reported. Inorganic macrocyclic or macrocyclic complexes of transition metals may serve in a better way than the aromatic nitro compounds as drugs, as they may have comparatively better solubility and show a lesser toxic effect.

Acknowledgements

Financial support from the Council for CSIR (Ref. No. 01(7329)/07/EMR-II) and DST (Ref. No. SR/S1/IC-35/2006), New Delhi, India is gratefully acknowledged.

Appendix A. Supplementary data

CCDC 278587 and 278586 contain supplementary crystallographic data for **2** and **3**. These data can be obtained free of charge via http://www.ccdc.cam.ac.uk/conts/retrieving.html, or from the Cambridge Crystallographic Data Centre, 12 Union Road, Cambridge CB2 1EZ, UK; fax: (+44) 1223-336-033; or e-mail: deposit@ccdc.cam.ac.uk. Supplementary data associated with this article can be found, in the online version, at doi:10.1016/j.poly.2008.06.035.

References

[1] (a) J.M. Lehn, Supramolecular Chemistry, VCH, Weinheim, Germany, 1995;
(b) T. Iwamoto, D.D. MacNicol, F. Tod, R. Bishop (Eds.), Comprehensive Supramolecular Chemistry, Pergamon Press, Oxford, 1996, p. 6. (Chapter 19);
(c) G.R. Desiraju, Nature 412 (2001) 397;
(d) M. Kawahara, M.K. Kabir, K. Yamada, K. Adachi, H. Kumagai, Y. Narumi, K.

Kindo, S. Kitagawa, S. Kawata, Inorg. Chem. 43 (2004) 92;
(e) B.H. Ye, M.L. Tong, X.M. Chen, Coord. Chem. Rev. 249 (2005) 545;
(f) A. Ray, D. Maiti, M. Ali, W.S. Sheldrick, H. Meyer-Figge, Indian J. Chem. A 44 (2005) 261 and references cited therein;
(g) A. Ray, M. Mijanuddin, R. Chatterjee, J. Marek, S. Mondal, M. Ali, Inorg. Chem. Commun. 9 (2006) 167 and references cited therein.
[2] (a) O. Kahn (Ed.), Magnetism: A Supramolecular Function, Kluwer, Dordrecht, 1996;
(b) M. Eddaoudi, D.B. Moler, H. Li, B. Chen, T.M. Reineke, M. O'Keeffe, O.M. Yaghi, Acc. Chem. Res. 34 (2001) 319;
(c) Y.R. Martin, M.H. Molina, F.S. Delgado, J. Pasan, C.R. Perez, J. Sanchiz, F. Lloret, M. Julve, Cryst. Eng. Commun. 4 (2002) 522;
(d) A. Ray, C.S. Hong, S. Mondal, M. Mukherjee, M. Ali, Inorg. Chem. Commun. 10 (2007) 527 and references cited therein.
[3] J. Černák, M. Orendáč, I. Potočňák, J. Chomič, A. Orendáčová, J. Skoršepa, A. Feher, Coord. Chem. Rev. 224 (2002) 51.
[4] (a) M. Verdaguer, A. Bleuzen, V. Marvaud, J. Vaissermann, M. Seuleiman, C. Desplanches, A. Scuiller, C. Train, R. Garde, G. Gelly, C. Lomenech, I. Rosenman, P. Veillet, C. Cartier, F. Villain, Coord. Chem. Rev. 190–192 (1999) 1023;
(b) D.H. Kim, J.E. Koo, C.S. Hong, S. Oh, Y. Do, Inorg. Chem. 44 (2005) 4383. and references cited therein.
[5] (a) H.Z. Kou, D.Z. Liao, P. Cheng, Z.H. Jiang, S.P. Yan, G.L. Wang, X.K. Yao, H.G. Wang, J. Chem. Soc., Dalton Trans. (1997) 1503;
(b) D.G. Fu, J. Chen, X.S. Tan, L.J. Jiang, S.W. Zhang, P.J. Zheng, W.X. Tang, Inorg. Chem. 36 (1997) 220;
(c) D. Ghoshal, A.K. Ghosh, T.K. Maji, J. Ribas, G. Mostafa, E. Zangrando, N. Ray Chaudhuri, Inorg. Chim. Acta 359 (2006) 593;
(d) D.J. Chesnut, J. Zubieta, Chem. Commun. (1998) 1707.
[6] (a) E. Colacio, J.M. Domínguez-Vera, M. Gazi, R. Kivekäs, J.M. Moreno, A. Pajunen, J. Chem. Soc., Dalton Trans. (2000) 505;
(b) M. Salah El Fallah, J. Ribas, X. Solans, M. Font-Bardia, J. Chem. Soc., Dalton Trans. (2001) 247;
(c) Z. Smékal, Z. Trávníček, J. Mroziński, J. Marek, Inorg. Chem. Commun. 6 (2003) 1395;
(d) Y.S. You, D. Kim, Y. Do, S.J. Oh, C.S. Hong, Inorg. Chem. 43 (2004) 6899;
(e) N.F. Curtis, H. Puschmann, Acta Crystallogr., Sect. C 60 (2004) m410.
[7] (a) M. Ali, A. Ray, W.S. Sheldrick, H. Mayer-Figge, S. Gao, A.I. Sahmes, New. J. Chem. 28 (2004) 412;
(b) A. Ray, D. Dutta, P.C. Mondal, W.S. Sheldrick, H. Meyer-Figge, M. Ali, Polyhedron 26 (2007) 1012.
[8] (a) D.I. Edwards, M. Dye, H. Crane, J. Gen. Microbiol. 76 (1973) 135;
(b) D.I. Edwards, in: C. Hansch (Ed.), Comprehensive Medicinal Chemistry, fifth 5th ed., vol. 2, Pergamon Press, New York, 1990, p. 725;
(c) D. Greenwood, Antimicrobial Chemotherapy, 13th ed., Oxford University Press, Oxford, UK, 1995;
(d) N.S. Guenay, G. Capau, N. Ulusoy, N. Ergene, G. Oetuek, D. Kaya, Farmaco 54 (1999) 826;
(e) S. Kasai, H. Nagasawa, M. Yamashita, M. Masui, H. Kuwasaka, T. Oshodani, Y. Uto, T. Inomata, S. Oka, S. Inayama, H. Hori, Bioinorg. Med. Chem. 9 (2001) 453;
(f) J.D. Maya, S. Bollo, L.J. Núñez-Vergara, J.A. Squella, Y. Repetto, A. Morello, J. Perie, G. Gauviere, Biochem. Pharmacol. 65 (2003) 999.
[9] (a) J.E. Biaglow, B. Jarabson, C.L. Greenstock, J. Raleigh Mol. Pharmacol. 13 (1977) 269;
(b) C. Viode, N. Bettache, N. Cenas, R. Luise Krauth-Siegel, G. Chauviere, N. Bakalara, J. Perie. Biochem. Pharmacol. 57 (1999) 549;
(c) S. Trinh, G. Reysset, Mutat. Res. 398 (1998) 55.
[10] (a) P.B. Roberts, W.A. Denny, B.F. Cain, Br. J. Cancer 40 (1979) 641;
(b) P.B. Roberts, R.F. Anderson, W.R. Wilson, Int. J. Radiat. Biol. 51 (1987) 641;
(c) W.R. Wilson, B.G. Siim, W.A. Denny, P.L. van Zijl, M.L. Taylor, D.M. Chambers, P.B. Roberts, Radiat. Res. 131 (1992) 257;
(d) T. Sugita, M. Masuoka, Y. Nishikawa, S. Nishimoto, L. Jhou, K. Sasai, T. Kagiya, Anticancer Drug Des. 7 (1992) 277.
[11] (a) K.A. Skov, N.P. Farrell, Int. Radiat. Biol. 52 (1987) 289;
(b) K.A. Skov, Radiat. Res. 112 (1987) 217;
(c) K.A. Skov, N.P. Farrell, Int. J. Radiat. Biol. 57 (1990) 947.
[12] G.E. Adams, I.R. Flockhart, C.E. Smithen, I.J. Stratford, P. Wardman, M.E. Watts, Radiat. Res. 67 (1976) 9.
[13] (a) R.P. Mason, in: W.A. Pryor (Ed.), Free Radicals in Biology, vol. V, Academic Press, New York, 1982, p. 161;
(b) P. Wardman, M.F. Dennis, S.A. Everette, K.B. Patel, M.R.L. Stratford, M. Tracy, in: C.C. Rice-Evans, B.B. Halliwell (Eds.), Biochemical Society Symposium, vol. 61, Portland Press, 1985, p. 171;
(c) P. Wardman, Environ. Health Persp. 64 (1985) 309.
[14] (a) J.H. Tocher, D.I. Edwards, Free Radical Res. Commun. 6 (1989) 39;
(b) J.H. Tocher, D.I. Edwards, Free Radical Res. Commun. 16 (1992) 19;
(c) J. Carbajo, S. Bollo, L.J. Núñez-Vergara, P.A. Navarrete-Encina, J.A. Squella, J. Electroanal. Chem. 494 (2000) 69;
(d) L.J. Núñez-Vergara, D. Farias, S. Bollo, J.A. Squella, Bioelectrochemistry 53 (2000) 103;
(e) J. Carbajo, S. Bollo, L.J. Núñez-Vergara, A. Campero, J.A. Squella, J. Electroanal. Chem. 531 (2002) 187.
[15] P. Comba, N.F. Curtis, G.A. Lawrance, A.M. Sargeson, B.W. Skelton, A.H. White, Inorg. Chem. 25 (1986) 4260.
[16] H. Lund, Cathodic reduction of nitro and related compounds, in: H. Lund, O. Hammerich (Eds.), Organic Electrochemistry, 4th ed., Marcel Dekker, New York, 2001, p. 379.
[17] P.C. Mondal, J. Electroanal. Chem. 570 (2004) 55.
[18] A. Ray, D. Maiti, W.S. Sheldrick, H. Meyer-Figge, S. Mondal, M. Mukherjee, M. Ali, Inorg. Chim. Acta 358 (2005) 3471.
[19] G. M. Sheldrick, SHELXL'97, Program for Crystal Structure Refinement, University of Gottingen, Germany, 1997.
[20] (a) A.G. Sharpe, The Chemistry of the Cyano Complexes of Transition Metals, Academic Press, London, 1976;
(b) K. Nakamoto, Infrared and Raman Spectra of Inorganic and Coordination Compounds, 4th ed., Wiley Interscience, New York, 1987.
[21] J.F. Willart, A. De Gusseme, S. Hemon, G. Odou, F. Danede, M. Descamps, Solid State Commun. 119 (2001) 501.
[22] A. Saleki-Gerhardt, J.G. Stowell, S.R. Byrn, G. Zografi, J. Pharm. Sci. 84 (1996) 318.
[23] N. Onodera, H. Suga, S. Seki, Bull. Chem. Soc. Jpn. 41 (1968) 2222.
[24] N. Shaikh, S. Goswami, A. Panja, X.Y. Wang, S. Gao, R.J. Butcher, P. Banerjee, Inorg. Chem. 43 (2004) 5908.
[25] M. Noel, K.I. Vasu, in: Mohan Primlani (Ed.), Cyclic Voltammetry and the Frontiers of Electrochemistry, Oxford & IBH Publishing Co. Pvt. Ltd., New Delhi, 1990.